

## Article

# Study of Overlying Rock Structure and Intensive Pressure Control Technology of Island Longwall Panel in Extra-Thick Coal Seams

Yaochuang Wang <sup>1</sup>, Pengkun Chen <sup>2</sup> and Shen Wang <sup>2,3,\*</sup><sup>1</sup> ZhongYun International Engineering Co., Ltd., Zhengzhou 450007, China<sup>2</sup> School of Energy Science and Engineering, Henan Polytechnic University, Jiaozuo 454003, China<sup>3</sup> Collaborative Innovation Center for Safe Production and Clean and Efficient Utilization of Coal, Jiaozuo 454003, China

\* Correspondence: wangshen@hpu.edu.cn

**Abstract:** In response to the severe occurrence of mining pressure in the fully mechanized top coal caving face of the extra-thick coal seam and the problem of strong rock pressure caused by the remaining coal pillars in the mining area on the isolated island fully mechanized top coal caving face, taking the 8102 isolated island working face of Tongxin Coal Mine as the background and by using methods such as on-site measurement and numerical simulation experiments, the characteristics of roof mining in the island longwall panel of extra-thick coal seams were analyzed. Establishing a mechanical model for the mining stress and overlying rock stress arch of an isolated working face, the mechanical characteristics of the isolated working face under special conditions were obtained. The results show that the longwall panel no. 8102 has an asymmetric long-arm T-shaped covering layer structure before mining and a C-shaped covering rock structure during mining, which will exacerbate the degree of mining pressure manifestation in the working face. Directional high-pressure hydraulic fracturing was implemented in the gob of longwall panel no. 8102, and the pressure reduction effect of the advance support section of the gob was obvious, ensuring the safety of the working face.



**Citation:** Wang, Y.; Chen, P.; Wang, S. Study of Overlying Rock Structure and Intensive Pressure Control Technology of Island Longwall Panel in Extra-Thick Coal Seams. *Processes* **2023**, *11*, 3083. <https://doi.org/10.3390/pr11113083>

Academic Editors: Raymond Cecil Everson, Feng Du, Aitao Zhou and Bo Li

Received: 6 September 2023

Revised: 19 October 2023

Accepted: 23 October 2023

Published: 26 October 2023



**Copyright:** © 2023 by the authors. Licensee MDPI, Basel, Switzerland. This article is an open access article distributed under the terms and conditions of the Creative Commons Attribution (CC BY) license (<https://creativecommons.org/licenses/by/4.0/>).

**Keywords:** extra-thick coal seam; strong rock pressure; island longwall panel; C-shaped overlying rock structure

## 1. Introduction

During the mining process of the fully mechanized top coal caving face in extremely thick coal seams, due to the large thickness of the coal seam extracted at one time, a large-scale mining space is formed, and the stable masonry beam structure is formed in the higher layers of rock layers, resulting in a strong rock pressure phenomenon in the fully mechanized top coal caving face. When there are residual coal pillars in the gob, the isolated island fully mechanized top coal caving face of the extra-thick coal seam where the pillar is extracted has a significant impact on its mining due to the combined influence of original rock stress and advanced support pressure.

On this basis, many scholars have conducted extensive research on the distribution law of mining-induced stress under different conditions and have achieved rich results.

Xingyun Ren [1] proposed to reduce the support pressure of the working face and protect the main roadway through roof cutting and pressure relief. Mingshi Gao [2] proposed a support plan that combines “active anchor cable support, hydraulic lifting support, and soft structure energy absorption”. Peng Wang [3] analyzed the deformation and instability characteristics of a composite roof coal roadway under different influencing conditions. Houqiang Yang [4] proposed and implemented the equidistant double bearing ring support technology. Zeng-Qiang Yang [5] proposed feasible methods for preventing rock burst using pressurized water jet technology. Xiaojie Yang [6] proposed the concept

of “cutting and reducing pressure on adjacent tunnel roof”. Xuyang Chen [7] studied the constitutive equation of the creep behavior of sandy mudstone and proposed corresponding solutions to improve the stability of the tunnel. Ming Ji [8] analyzed the radial variation of stress and displacement in tunnel surrounding rock.

Yuxin Yuan [9] proposed thick anchor crossing boundary support under strong mining conditions and its engineering application. Deyu Qian [10] revealed the deformation and damage characteristics and distribution law of the surrounding rock of a stress-intensive roadway. Kai Wang [11] analyzed the use of microcrack grouting under high rock pressure conditions to quantitatively describe the changes in grout permeability distance and crack opening. Yunhai Cheng [12] proposed to reduce the impact of strong dynamic pressure on the roadway floor by changing the energy accumulation of the roadway floor. Jolfaei S [13] analyzed a large database and found that among the parameters that affect borehole fracture, the internal friction angle of the rock has the greatest impact on the fracture size. Jingxuan Yang [14] proposed measures to prevent strong rock using water-filled deep hole restricted blasting technology. Rui Gao [15] reveals the combined effect of a gob side relief zone and OCP stress concentration on final stress. Lu Chen [16] proposed a new type of energy-absorbing anchor rod with a small consumption of energy stored under high stress.

In the case of extremely thick coal seams, most previous studies have reflected the law of rock pressure behavior under a single condition. Therefore, this paper analyzes the roof structure of the island-shaped comprehensively placed working face of the extra-thick coal seam, simulates the mining stress and overburden rock stress arch of the working face for the special situation of the longwall panel no. 8102 of Tongxin Coal Mine, and puts forward the key technology of controlling the roof in the island-shaped comprehensively placed working face of the extra-thick coal seam on the basis of the key technology of controlling the roof of the extra-thick coal seam. The reliability of this simulation is verified based on on-site observation results.

## 2. Roof Structure of Island Longwall Panel in Extra-Thick Coal Seams

### 2.1. Engineering Geological Conditions

Located in the southwest of Datong City (Figure 1), Tongxin Coal Mine is 14.29 km from east to west and 10.36 km from south to north. The isolated longwall panel no. 8102 is located on the east side of the coal mining area no. 1. The eastern part is a solid coal area, the northern part is an 8103 goaf, the western part is a three-panel roadway, and the southern part is an 8101 goaf. Due to the fact that the adjacent working face 8102 has already been mined out, and a 6 m coal pillar has been left behind in the goaf, a situation of isolated working faces with goafs on both sides has been formed. The schematic diagram of the working face position is shown in Figure 2.

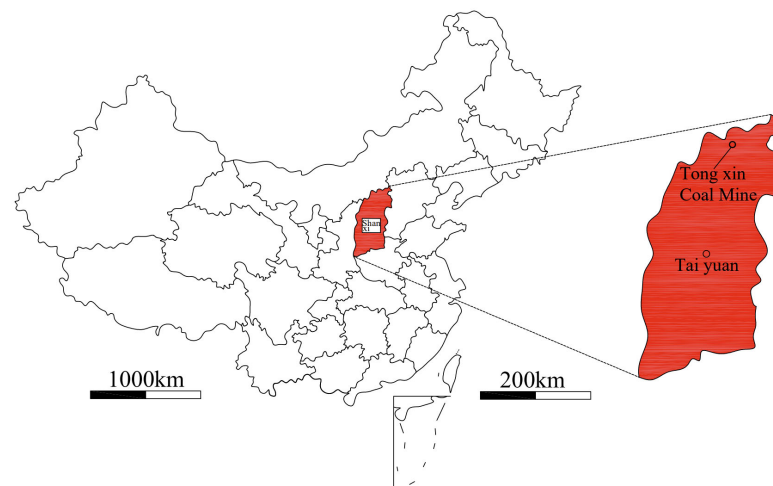


**Figure 1.** Location map of Tongxin Coal Mine.

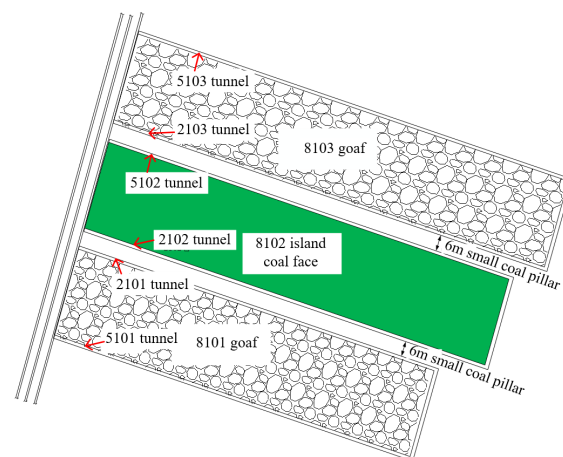


**Figure 2.** Principle of automatic hydraulic bracket following machine.

The burial depth of longwall panel no. 8102 is 437.1–491.6 m, with an average coal thickness of 17 m. This coal seam is a semi-dark type with a middle layer of semi-bright coal, which is brittle and fragile. Overall, the coal seams in this working face have a relatively high floor near the panel roadway and cutting hole, while the middle floor is relatively low. There are 5–10 dirt bands in the coal seam, and the lithology is generally kaolinite, sandy mudstone, and carbonaceous mudstone, with occasional siltstone or fine sandstone. The dip angle of the coal seam is  $0\sim 4^\circ$ , with an average of  $1^\circ$ . The overburden of longwall panel no. 8102 mainly consists of fine sandstone, siltstone, and medium sandstone, with good integrity, high hardness, and high strength. The rock column diagram of longwall panel no. 8102 is shown in Figure 3. There are multiple layers of thick and high-strength sandstone layers distributed in the range of 100 m above the working face.

The mining roadway of longwall panel no. 8102 is a rectangular roadway. Within it, the excavation width of Lane 2102 is 5500 mm, the height is 3700 mm, the tunnel section is  $20.35\text{ m}^2$ , and the total length is 1822.66 m. The excavation width of Lane 5102 is 5200 mm, the height is 3950 mm, the tunnel section is  $20.54\text{ m}^2$ , and the total length is 1831.05 m. The excavation width of 8102 top extraction roadway is 4200 mm, the height is 2700 mm, the roadway section is  $11.34\text{ m}^2$ , and the total length is 1827.38 m. The cross-sectional diagram of the 8102 mining roadway is shown in Figure 4.

## 2.2. Full Mining Conditions on Both Sides of the Isolated Working Face

### (1) History of adjacent roadway mining

After the excavation of the working face, the cracks in the overlying rock gradually develop from bottom to top, with the lower rock layer stabilizing first and the surface rock layer stabilizing later. If the surface rock layer area is stable, then it can be inferred that the activity of the lower rock layer has stabilized. The 8101 working face was completed in 2010, about 8 years before this study. The 8103 working face was completed in 2015, about 3 years before this study. The adjacent working face 8102 has already been mined out, resulting in an isolated island working face with both sides being mined out.

### (2) Settlement status of overlying rock

Through on-site research, it was found that the longwall panel no. 8102 has the following crack characteristics: ① there are both tension-type cracks and shear cracks on the surface; ② the direction of most of the cracks is roughly related to the contour of the working face of seams 3–5 #, indicating that the cracks were caused by the mining of seams 3–5 #; ③ in the early stage, some cracks were filled, but in the later stage, the cracks began to propagate, partly due to atmospheric precipitation and partly due to crack activation; ④ some cracks become closed cracks, which may be formed during the mining process of the overlying coal seam and closed due to the mining of coal seams 3–5. In addition, some

tension joints closed due to the effects of secondary mining. Figure 5 shows the distribution of the investigated fractures: workings 8101 and 8103 on either side of workings 8102 were completed in October 2010 and March 2015, respectively. It has been at least 8 years since then, and it can be inferred that the overlying rock activity has tended to be stationary and formed new overlying rock structures.

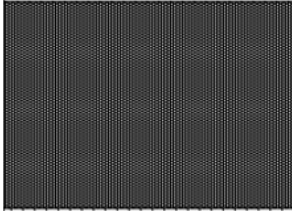
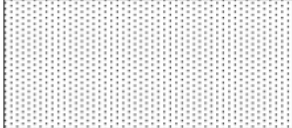
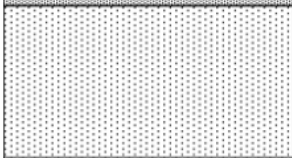
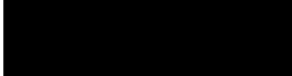
Columnar	Thickness/m	Buried depth/m	Rock properties
	1.60	375.20	Coarse grained sandstone
	19.30	394.50	Siltstone
	10.90	405.40	Glutenite
	1.10	406.50	Fine grained sandstone
	17.28	423.78	Glutenite
	1.90	425.68	Fine grained rock
	2.36	428.40	Fine grained sandstone
	10.27	438.31	Interbedded mudstone and sandstone
	2.00	440.31	No.4 coal
	3.44	443.75	Siltstone
	4.20	447.95	Fine grained sandstone
	7.00	454.95	Coarse grained sandstone
	3.65	458.60	Interbedded mudstone and sandstone
	4.53	463.13	Sandy mudstone
	1.80	464.93	No.2 coal
	0.90	465.84	Carbonaceous mudstone
	18.59	484.43	No.3-5 coal

Figure 3. Rock stratum histogram of longwall panel no. 8102.

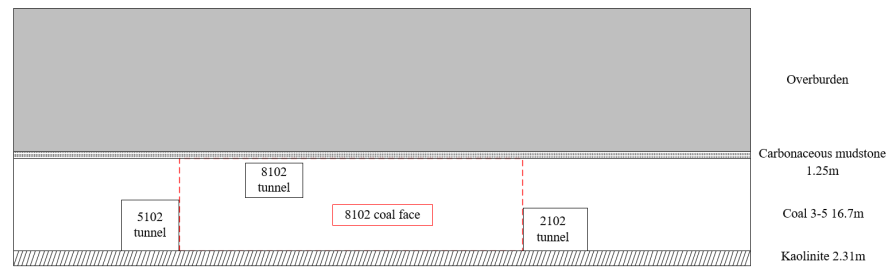


Figure 4. Section diagram of 8102 mining roadway.

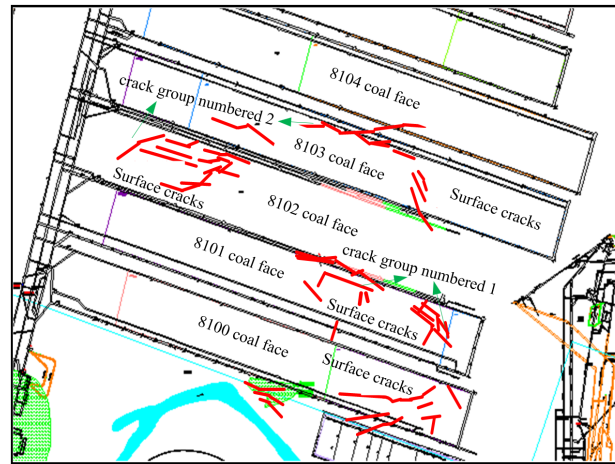


Figure 5. Crack investigation map.

It is speculated that the crack group numbered 1 in Figure 5 is a tension-type crack group that can be caused by the mining of working face 8101, while the crack group numbered 2 is caused by the joint mining of working faces 8101, 8103, and 8104. The distance between crack group 1 and the edge of working face 8101 is about 280 m, indicating that the fracture angle is approximately:

$$\phi = 90^\circ - \arctan(D/H) = 90^\circ - \arctan(280/484) = 59.95^\circ \quad (1)$$

The calculation principle of crack angle is shown in Figure 6. From this, it can be inferred that the overlying rock structure characteristics of a panel working face are inclined along the working face.

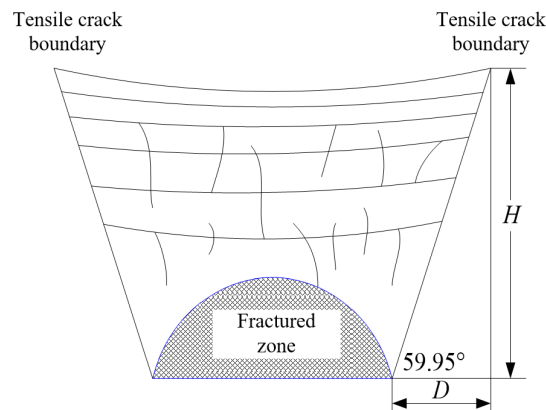


Figure 6. The influence range and structural diagram of the overlying rock along the dip after mining in a panel working face.

In addition, the structural characteristics of the stratigraphy overlying strata on the existing 8101 working face are inferred based on the discovered surface cracks. From Figure 6, it can be seen that ① the cracks on one side of the 8101 working face are cut along the direction of the 8101 roadway; ② the development of crack groups in the area near the main roadway of longwall panel no. 8102 indicates that after multiple mining impacts, there are many mining cracks in the overlying rock here; ③ the cracks on one side of the 8103 working face are mostly developed in the middle of the 8103 working face and near the junction of the 8103–8104 working face, and the distribution of cracks in the inclined direction shows asymmetric characteristics; ④ there are significantly more strike fractures than dip fractures, indicating that across the width of this working face, there are fewer developed dip fractures due to the hard and complete overlying rock.

This suggests that the longwall panel no. 8102 was mined with a longer length of overhanging roof along the direction of the workings, and if it suddenly breaks, there is a high possibility of causing strong impact on the working face.

Based on the above analysis, the following results can be summarized: the overlying rock structure of longwall panel no. 8102 is asymmetric, with a longer cantilever structure on the side near 8103 and a relatively shorter cantilever structure on the side near the 8101 working face. The near absence of inclined cracks in the overlying rock under these working face width conditions indicates the length of the hard rock strata suspended during the advance of the working face.

### 2.3. Full Mining Discrimination on Both Sides of Longwall Panel No. 8102

In order to analyze the temporal and spatial movement characteristics of the overlying rock strata of the Tongxin Coal Mine, the movement status of the underlying strata can be inferred from the surface subsidence law. Therefore, based on the mining subsidence characteristics of the 8105 working face, the spatiotemporal movement characteristics of the overlying strata in a panel can be inferred.

The 8105 working face belongs to a level northern area, with an average elevation of 797 m. The working face is a small anticline structure, with a gentle slope of 1–3° on both wings of the anticline. The eastern part of the working face is a solid coal area. The northern part is the 8106 working face, which has been mined out; There are three main alleys in the western region. The southern part is the 8104 working face.

The basic structural form of the mine field is a monocline trending northeast and tilting northwest, with a stratigraphic dip angle of 3–10° generally, and the southeast and south coal seam outcrops become steeper, reaching 30–80° and local vertical inversion; There are few faults, with a small amount of wide and gentle folds and collapse columns.

In addition, there are oil lampblack intrusions on both the east and west sides of the mine, which have a significant impact on the coal quality of the coal seam. There is moderate to simple construction complexity.

The roof, floor, and solid rock of coal seams are generally semi-hard to hard rocks with good engineering geological conditions, belonging to a simple type. The gas content is usually low but locally high. The specific conditions of the top and bottom plates of the 8105 working face are shown in Table 1. The mining parameters of the 8105 working face in Tongxin Coal Mine are shown in Table 2.

**Table 1.** Lithological characteristics of the top and bottom plates of working face 8105.

Name of Top and Bottom Plates	Rock Name	Thickness (m)	Lithological Characteristics
Main roof	Silty fine sandstone and gravelly gritstone	11.39	Grayish white gravelly gritstone, mainly composed of quartz, followed by feldspar, mica, and dark minerals, which is of subangular shape, poor sorting, and hard structure

**Table 1.** *Cont.*

Name of Top and Bottom Plates	Rock Name	Thickness (m)	Lithological Characteristics
Immediate roof	Siltstone and carbonaceous mudstone	3.35	Siltstone: horizontal bedding and coal chips; carbonaceous mudstone: block shaped, easily stains hands, containing plant stem and leaf fossils
Immediate floor	Mudstone	1.94	It is dark gray, massive, loose, and fragile, containing a small amount of siltstone

**Table 2.** Mining parameters of 8105 working face.

Name	Technical Parameter Values	
Working surface parameters	Strike length $D_3$	1757 m
	Inclination length $D_1$	200 m
Boundary mining depth	Downhill direction $H_1$	460.0 m
	Uphill direction $H_2$	470.0 m
	Open-off cut $H_3$	400.0 m
	Stop line $H_4$	490.0 m
Average dip angle of coal seam	1~3°	
Coal seam thickness	13.12–22.85 (average 16.85)	
Working face direction	107°	
Working face inclination	197°	
Coal-mining methods	Comprehensive mechanized coal mining	
Roof management methods	Total collapse method for roof management	

The 8105 working face surface movement and deformation observation station is equipped with three observation lines, A, B, and C. One main section-monitoring line of strike, two dip observation lines, eighty-four deformation-monitoring points, eight control points, and ninety-two total observation points are set. The average distance between observation points on the observation line is taken as 30 m. Taking into account the parameters of ground fissures, surface morphology damage, and surface movement and deformation, the following conclusions are drawn:

① According to the on-site investigation of surface cracks in a certain area, it can be seen that the surface cracks extend relatively far, with most of them developing along the advancing direction but exhibiting discontinuous characteristics. Fracture development in the direction of the working face is relatively small, suggesting that the impact of mining on the surface is limited in a given area due to the hard rock formations in the strata.

② According to on-site research, no subsidence basins were clearly observed due to the influence of terrain.

③ According to the observation of surface rock movement in the 8105 working face with one side of the gob, the maximum subsidence is only 4.994 m, and the expected subsidence coefficient is 0.4. This indicates that under the geological structure characteristics and mining conditions of a panel, one side of the gob is not fully mined after mining, and the strata have not fully settled.

#### 2.4. Evolution of Overlying Rock Spatial Structure during the Mining Process of Fully Mechanized Top Coal Caving Face in Extra-Thick Coal Seams

For multiface mining, whether the overlying rocks in two adjacent gob areas can form an interactive spatial structure mainly depends on the width of the coal pillar between the two. A large coal pillar can effectively isolate the connection between the overlying rock fractures in the gob. Generally, a coal pillar of more than 20 m between the working faces can isolate the movement of the overlying rock between the two working faces. Therefore, when the coal pillar of the working face is smaller than a certain value, the overlying rock between the working faces will form a collaborative movement, forming an interactive spatial structure. A small coal pillar 6 m wide was left between the 8102 face and the section of the mining area on both sides. Therefore, this small coal pillar cannot separate the overlying rock structure of the longwall panel no. 8102 from the overlying rock structure above the gob areas on both sides but rather forms an interactive spatial structure.

Generally, the spatial structure of the overlying rock in the mining area is divided into four types: the overlying rock spatial structure during the advancement of the surrounding solid coal working face, the overlying rock spatial structure during the advancement of the working face with one side of the gob, the overlying rock spatial structure during the advancement of the isolated island working face with both sides of the gob, and the overlying rock spatial structure of the isolated island working face with four sides of the gob. The longwall panel no. 8102 is an isolated island working face with gob on both sides, and its spatial structure shows a “C” shape.

The formation process of C-type: this type of stope is an isolated working face left behind by skip mining. In recent years, the roadway support of the synthesized isolated working face has become a very difficult problem. Some working faces have advanced support pressure that affects a distance of up to 120 m, and roadway repair engineering has become a “bottleneck” for advancing the working face. There is still a problem of large-scale peeling in the deep working face. Figure 7 shows the spatial structure of the overlying rocks in this type of mining area. The rock layers above the main roof slabs of the three mining areas have been connected into a similar “C”-shaped spatial structure, and the large-scale movement of the “C”-shaped spatial structure is the main reason why the influence distance of the pressure on the overhanging support in the isolation workings is 2–3 times larger than that of the ordinary workings [17].

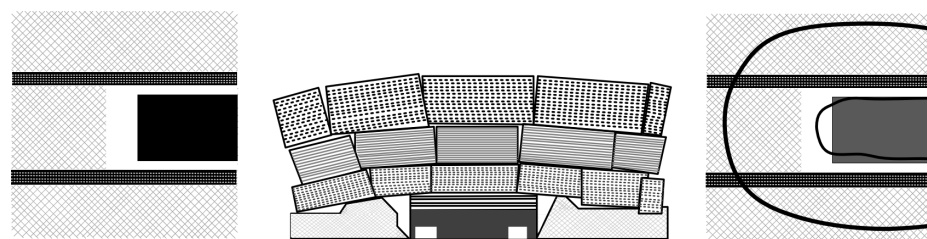


**Figure 7.** Schematic diagram of the spatial structure of the C-shaped overlying rock.

According to surface subsidence observation data and surface crack research, the insufficient settlement of the gob on both sides indicates that the longwall panel no. 8102 will form a long-arm T-shaped structure, and the asymmetric distribution of cracks indicates that the overlying rock of longwall panel no. 8102 will form an asymmetric longwall T-shaped structure (Figure 8a,b). The rock pressure manifestation under this structure is the most severe, equivalent to the cantilever of hard rock being completely above the working face. During the mining period, the basic roof of the longwall panel no. 8102 will form a C-shaped overlying rock structure.

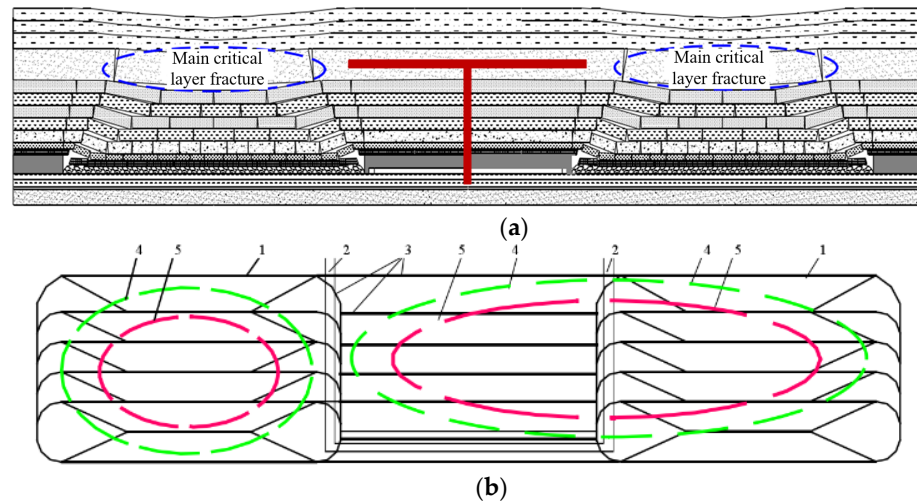


**Figure 8.** Schematic diagram of T-shaped overlying rock spatial structure. (a) Schematic diagram of symmetrical short-arm T-shaped overlying rock structure section. (b) Schematic Plan of Symmetrical Short-Arm T Overburden Structure.

### 3. Numerical Simulation of Mining Stress and Overlying Rock Stress Arch in Working Face

Longwall panel no. 8102 is an isolated island working face, and its advanced coal body stress state and overlying rock stress state are closely related to the possibility of dynamic disasters. This time, ABAQUS numerical calculation software was used to calculate the distribution of mining stress in the working face no. 8102, taking into account the impact of adjacent gobs (8100, 8103 gobs, and the overlying coal seam gob 14 #), providing a basis for evaluating the risk of dynamic disasters.

#### 3.1. Numerical Simulation Establishment

A three-dimensional numerical model was established using ABAQUS/CAE pre-processing software, the geometric model is shown in Figure 9, and the mesh model is shown in Figure 10. The Mohr–Coulomb softening model can be defined directly in ABAQUS/CAE. Among them, the width dimensions of each working face and coal pillar in the coal seams 3–5 # are established based on the actual dimensions. In order to reduce the computational complexity, appropriate selection of the forward length of the working face is necessary to ensure representativeness. Finally, the forward length of the working face was chosen to be 400 m.

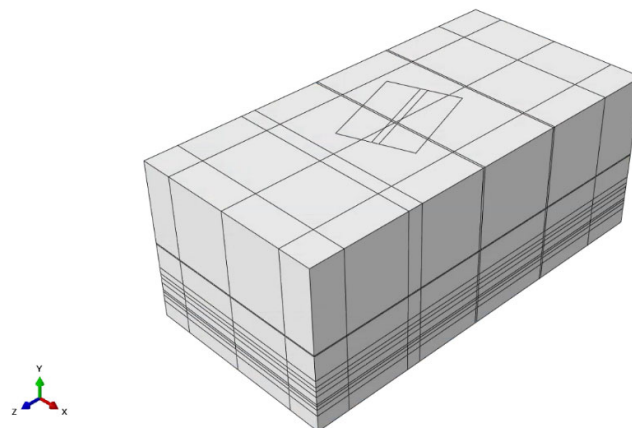


**Figure 9.** Geometric model.

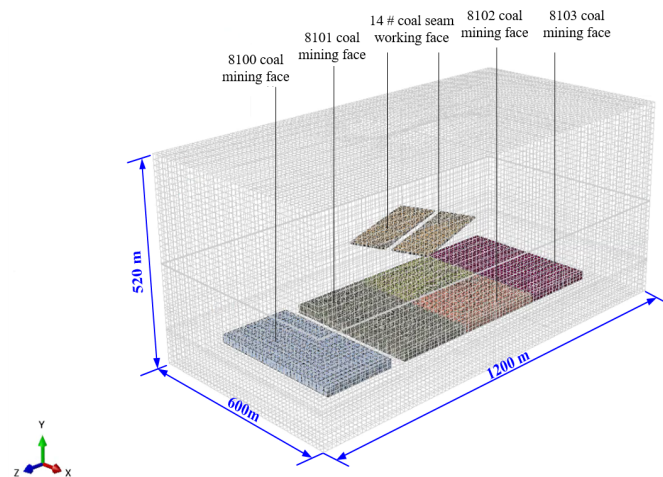


**Figure 10.** Grid model.

By comparing the corresponding relationship between the gob of coal seam 14 # and the longwall panel no. 8102, it can be seen that: ① the angle between the direction of coal seam 14 # working face and the direction of the longwall panel no. 8102 is about  $48^\circ$ ; ② 15–30 m wide coal pillar is left in the 4-seam mining area; ③ the width of the gob in coal seam 14 # is approximately 100 m. Based on the above spatial relationships and geometric parameter conditions, in this numerical simulation, the angle between the working face direction of seam 14 # and the direction of longwall panel no. 8102 is about  $48^\circ$ , and the working face width of seam 14 # is 100 m, and 20 m coal pillars are reserved in the section. To reduce computational complexity and minimize the impact of boundary conditions, only two working faces of coal seam 14 # are considered. The coal seam 14 # working face spans above the 8102 and 8101 working faces.

The numerical model is 1200 m long, 600 m wide, and 520 m high. It is divided into about 331,600 hexahedron elements. The element type is C3D8, that is, a three-dimensional eight-node full integration element. In the model, the displacement constraint in the x-direction of the two boundary interfaces perpendicular to the x-direction is  $U1 = 0$ . The z-direction displacement constraint of the two boundary interfaces perpendicular to the z-direction is  $U3 = 0$ . The y-direction displacement constraint of the bottom surface perpendicular to the y-direction is  $U2 = 0$ .

### 3.2. Numerical Simulation Parameters

#### (1) Constitutive model of rock strata

Dynamical problems involve the transfer of energy from elastic energy to kinetic energy in the subsurface. Based on the stress and strain components, the elastic energy in a solid finite element can be calculated. Therefore, selecting a relatively accurate model to reflect the stress–strain relationship and energy characteristics of rocks is the key to simulating roof impact problems. In addition, for numerical simulation, the final output parameter values were evaluated and determined from numerical simulation results and field observations. Therefore, rock deformation needs to be carefully considered in numerical simulations again.

In this study, the Mohr–Coulomb strain-softening model is selected to describe the rock deformation behavior caused by the unloading effect of underground coal seam mining. The stress–strain relationship in the elastic phase of the Mohr–Coulomb strain-softening model is the same as that of the Mohr–Coulomb model, while the stress–strain relationship in the plastic stage is different, as shown in Figure 11. In the Mohr–Coulomb model, the stress component after the yield point increases with the increase in the strain component, which is called the ideal elastic–plastic model. In the Mohr–Coulomb strain-softening model, the cohesion, friction angle, and tensile strength decrease with increasing plastic

strain. In Figure 11,  $U_1$  represents the elastic energy at the yield point, while  $U_2$  and  $U_3$  represent the elastic energy in the post-peak phase of the ideal elastic–plastic and strain-softening models, respectively. Obviously, the Mohr–Coulomb model cannot reflect the actual deformation behavior and elastic energy release, while the Mohr–Coulomb strain-softening model can describe the softening behavior and elastic energy release process ( $U_1 > U_3$ ).

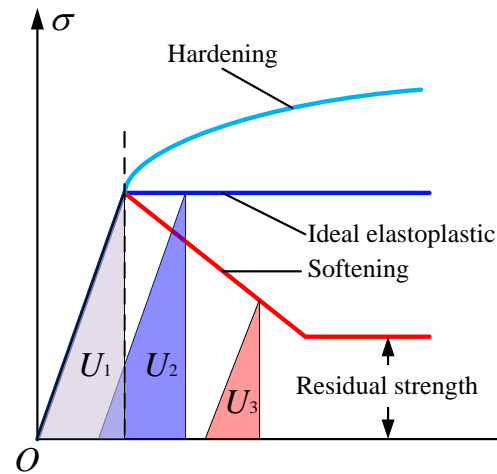


Figure 11. Schematic diagram of the Mohr–Coulomb model and its softening model.

In the elastic stage, the total strain tensor is equal to the elastic strain tensor, as follows:

$$\boldsymbol{\varepsilon} = \boldsymbol{\varepsilon}^e \quad (2)$$

In the post-peak phase, the total strain tensor is equal to the sum of the elastic and plastic strain tensor. The plastic strain tensor can be divided into two parts: the plastic shear strain tensor and the plastic tensile strain tensor. Therefore, the total strain tensor can also be expressed as:

$$\boldsymbol{\varepsilon} = \boldsymbol{\varepsilon}^e + \boldsymbol{\varepsilon}^{ps} + \boldsymbol{\varepsilon}^{pt} \quad (3)$$

The shear yield function  $F^s$  in the Mohr–Coulomb softening model is expressed as:

$$F^s = \sigma_1 - \sigma_3 N_\phi + 2c \sqrt{N_\phi} \quad (4)$$

In the equation,  $\sigma_1$  is the maximum principal stress,  $\sigma_3$  is the minimum principal stress,  $c$  is the cohesion force, and  $\phi$  is the friction angle.

The tensile yield function  $F^t$  is:

$$F^t = \sigma_t - \sigma_3 \quad (5)$$

In the formula,  $t$  is the tensile strength.

The shear plastic potential function  $g^s$  is based on the noncorrelated flow rule, while the tensile plastic potential function  $g^t$  is based on the correlated flow rule.

$$g^s = \sigma_1 - \sigma_3 N_\phi \quad (6)$$

$$g^t = -\sigma_3 \quad (7)$$

When shear failure occurs, the increase in shear plasticity can be calculated as:

$$\Delta \varepsilon_i^{ps} = \lambda^s \frac{\partial g^s}{\partial \sigma_i} \quad (8)$$

When tensile failure occurs, the increase in tensile plasticity can be calculated as:

$$\Delta \varepsilon_i^{pt} = \lambda^t \frac{\partial g^t}{\partial \sigma_i} \quad (9)$$

In the above equation,  $\Delta \varepsilon_i^p$  is the plastic strain increment, and  $\lambda^s$  and  $\lambda^t$  are undetermined coefficients.

By introducing Equation (6) into Equation (8), the plastic strain increment component  $\Delta \varepsilon_i^p$  under shear failure can be calculated as follows:

$$\begin{cases} \Delta \varepsilon_1^{ps} = \lambda^s \\ \Delta \varepsilon_2^{ps} = 0 \\ \Delta \varepsilon_3^{ps} = -\lambda^s N_\phi \end{cases} \quad (10)$$

For isotropic materials, the relationship between the principal stress increment and the principal strain increment according to the generalized Hooke's law is:

$$\begin{cases} \Delta \sigma_1 = \alpha \Delta \varepsilon_1 + \beta (\Delta \varepsilon_2 + \Delta \varepsilon_3) \\ \Delta \sigma_2 = \alpha \Delta \varepsilon_2 + \beta (\Delta \varepsilon_1 + \Delta \varepsilon_3) \\ \Delta \sigma_3 = \alpha \Delta \varepsilon_3 + \beta (\Delta \varepsilon_1 + \Delta \varepsilon_2) \end{cases} \quad (11)$$

In the formula,  $\sigma_1$ ,  $\sigma_2$ , and  $\sigma_3$  are the maximum, middle, and minimum principal stress increments, respectively;  $\varepsilon_1$ ,  $\varepsilon_2$ , and  $\varepsilon_3$  are the maximum, middle, and minimum principal strain increments, respectively;  $\alpha$  and  $\beta$  are elastic constants, which can be calculated by Young's modulus and Poisson's ratio.

According to Equations (3), (9) and (10), the stress component under shear failure mode can be updated to:

$$\begin{cases} \sigma_1^N = \sigma_1^O - \lambda^s (\alpha - \beta N_\phi) \\ \sigma_2^N = \sigma_2^O - \beta \lambda^s (1 - N_\phi) \\ \sigma_3^N = \sigma_3^O - \lambda^s (\beta - \alpha N_\phi) \end{cases} \quad (12)$$

In the equation,  $\sigma_i^N$  and  $\sigma_i^O$  are the new and old stress states,  $i = 1, 2$ , and  $3$ , respectively. Similarly, the stress component under tensile failure mode can be updated to:

$$\begin{cases} \sigma_1^N = \sigma_1^O + \lambda^t \beta \\ \sigma_2^N = \sigma_2^O + \lambda^t \beta \\ \sigma_3^N = \sigma_3^O + \lambda^t \alpha \end{cases} \quad (13)$$

The initial shear expansion angle is taken as  $1/3-1/2$  of the friction angle. In ABAQUS, the strain-softening function is defined as a table function of. The cohesion and friction angle decay linearly with increasing plastic strain. When the plastic strain reaches  $5 \times 10^{-3}$ , the cohesion and friction angle decay to the original 25%. The attenuation slope is determined by displacement back analysis. Afterwards, the cohesion and friction angle remain unchanged, characterizing the residual strength of the rock.

## (2) Bedding model and parameters

The mechanical behavior of bedding is divided into tangential and normal behaviors, as shown in Figure 12. In ABAQUS, the Coulomb friction model is used to simulate the tangential behavior of bedding. The normal behavior is defined as a hard contact model with initial tensile strength. Bedding stiffness is determined using the penalty function method; therefore, when the bedding shear stress is less than the shear strength, ABAQUS is also required to give an allowable initial elastic slip that is less than 0.05 times the characteristic length of the member. Typically, the tensile strength of rock formations is significantly lower than that of rocks and is often difficult to measure accurately. The initial tensile strength is set to 0.01 MPa and the initial coefficient of friction is set to 0.30.

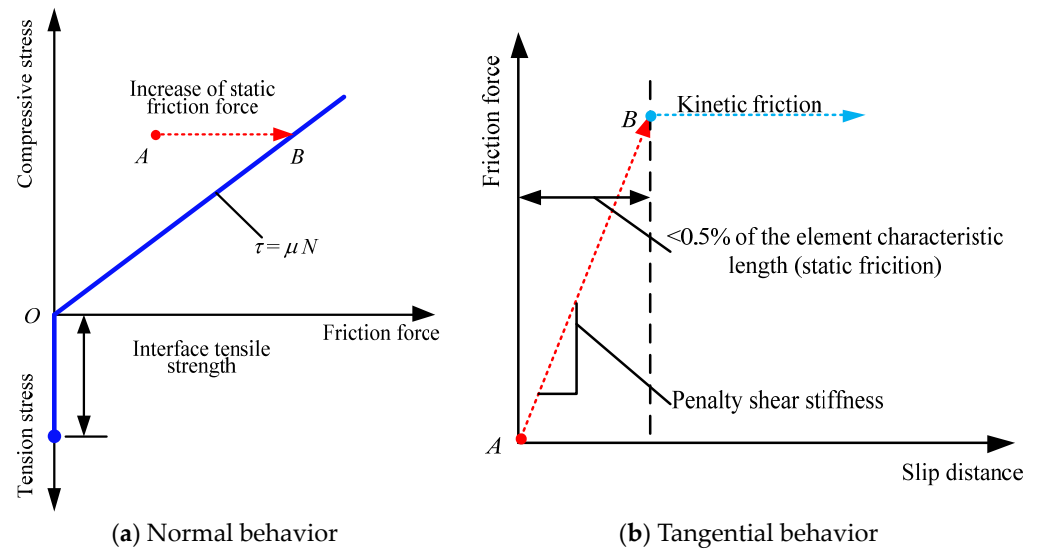


Figure 12. Mechanical behavior of bedding.

### (3) Gob model

The compression process of gob is an important simulation part in the numerical simulation of longwall mining, which will significantly affect the settlement and migration laws of overlying rocks. In this simulation, the gob model proposed by Salamon in 1991 [18] was used. In this model, the vertical stress in the extraction zone increases with increasing vertical strain as shown in the following equation:

$$\sigma_v = \frac{E_{gob}\varepsilon_v}{\varepsilon_{gob} - \varepsilon_v} \quad (14)$$

In the formula,  $E_{gob}$  is the initial deformation modulus of the gob, and  $\varepsilon_{gob}$  is the ultimate vertical strain of the gob.

The initial values of deformation modulus and ultimate vertical strain are  $E_{gob} = 3.5$  MPa and  $\varepsilon_{gob} = 0.5$ , respectively. Therefore, according to the above equation, the gob is a nonlinear elastic material. The bulk modulus of the gob continues to increase with the volume strain of the gob, and the bulk modulus can be calculated by the following formula:

$$K = \frac{1.75}{0.5 - \varepsilon_z} \quad (15)$$

In the formula,  $\varepsilon_z$  is the vertical strain component of the gob unit.

As the longwall face advances, collapse zones, fracture zones, and continuous deformation zones are formed above the coal seam. The height of the collapse zone gradually decreases as the veinstone filling in the mining airspace is gradually compressed. The final compression height of the collapse zone can be calculated as:

$$h_c^f = \frac{100M}{2.1M + 16} \pm 2.5 \quad (16)$$

In the formula,  $h_c^f$  is the final compression height of the collapse zone, and  $M$  is the mining thickness. According to Equation (16), the final compression height of longwall panel no. 8102 is 31.48–36.48 m.

The coefficient of collapse and expansion in the collapse zone is:

$$k_c = \frac{H_c}{H_r} \quad (17)$$

In the formula,  $k_c$  is the coefficient of collapse and expansion,  $H_c$  is the height of the collapse zone, and  $H_r$  is the direct top height before collapse.

As the gob is compacted, the coefficient of fragmentation and swelling in the collapsed zone gradually decreases. It is assumed that the initial and final breakup coefficients are 1.25 and 1.05. The initial height of the gob can be calculated as:

$$h_c^i = \frac{k_c^i}{k_c^f} h_c^f \quad (18)$$

According to Equation (18), it is between 37.48 and 43.43 m, and the average value of 40.46 m is taken in this numerical simulation.

The above gob constitution is programmed using the user subroutine UMAT and executed in ABAQUS/Standard.

#### (4) Simulation method for excavation of working face

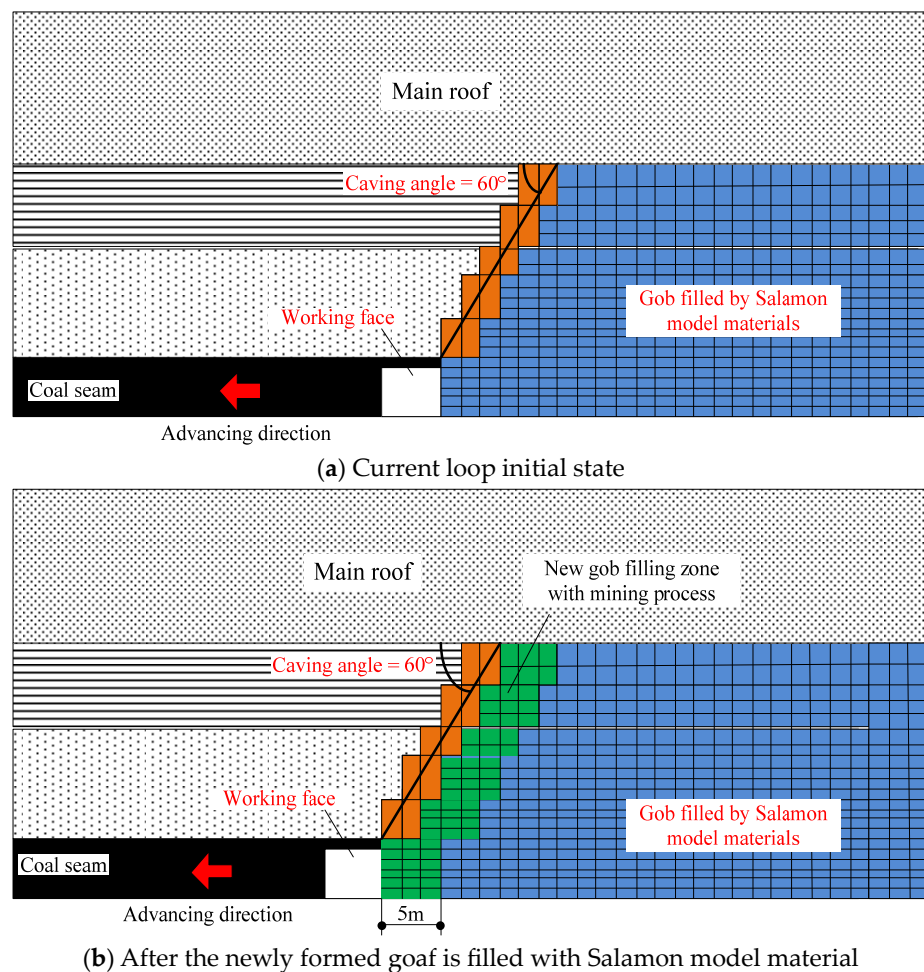
The longwall mining process was simulated using the “Static/General” solver mode and the “Standard” solver in ABAQUS. The matrix storage of finite element equation solving is asymmetric. The solution method is Newton–Raphson’s method. In order to improve the convergence of nonlinear analysis, the viscosity coefficient of the C3D8 element is set to 0.0001. The global numerical damping is set to 0.05.

In the simulation software, the coal seam 14 # working face, 8101 working face, 8200 working face, 8103 working face, and longwall panel no. 8102 were excavated in sequence. The stress distribution in an elastic body is independent of the loading or unloading path. However, the loading and unloading paths have a significant effect on the stress–strain evolution of the plasticizer. Therefore, the failure and deformation of the roof rock layer are influenced by the mining sequence. Therefore, implementing the mining process in ABAQUS is the most necessary in the actual mining process of coal mines. Figure 13 shows a typical cycle in the numerical mining process. The advance distance of each step in the simulation should be less than the main roof rupture distance of 12–32 m to avoid its influence on the main roof rupture behavior and pressure change characteristics. Therefore, the mining step length of one cycle was set to 5 m; the material properties of the extraction zone were converted to the Salamon model at a rate of 5 m/cycle.

#### (5) Numerical simulation verification

In order to analyze the stress–strain characteristics of coal under different surrounding rock pressure conditions, lime fine Taiyuan Group 3–5 coal samples were taken in Tongxin Coal Mine and processed into standard specimens along the coal seam layer direction [19], with a length of 100 mm and a diameter of 50 mm. Due to the low strength of the coal seam in the working face, it is not possible to drill cylindrical samples. The coal samples collected on site are processed into cylindrical samples.

The processed standard coal and rock samples were numbered, the dimensions were measured with a vernier caliper, and they were weighed with an electronic balance. The physical and mechanical parameters of coal and rock were obtained through the RMT-150B rock mechanics testing system, and uniaxial compression tests were conducted on the processed coal and rock samples. Some coal samples and testing equipment are shown in Figure 14.

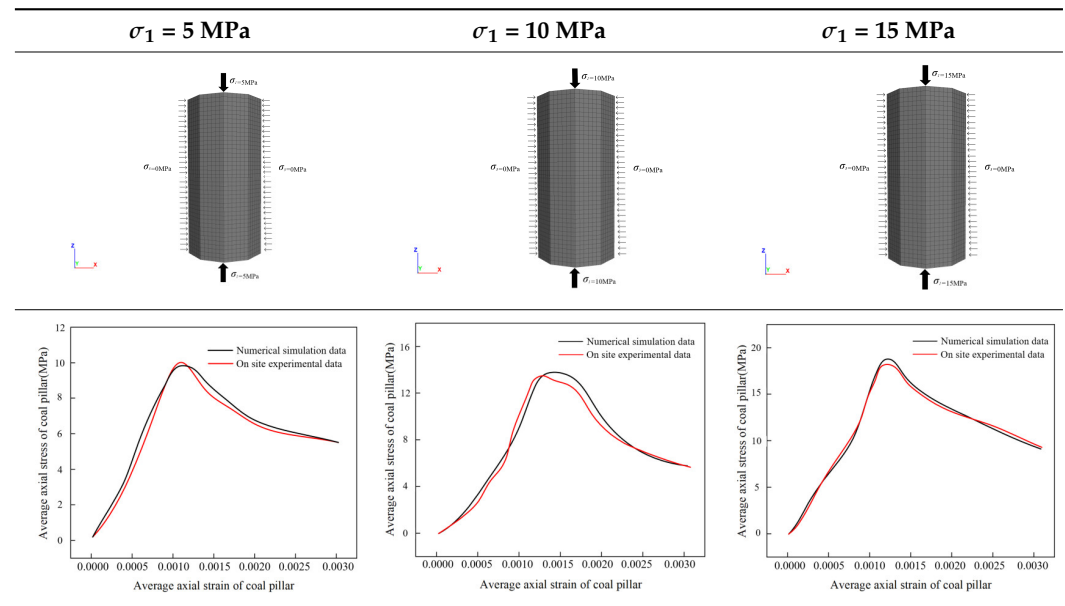


**Figure 13.** Schematic diagram of excavation simulation method for working face.



**Figure 14.** Partial coal samples and testing equipment.

At the same time, ABAQUS software is used to simulate the scenario of uniaxial compression of coal samples. Firstly, the displacement of the model in the normal direction is limited, and the displacement in the vertical normal direction is also limited. Then, the vertical displacement at the bottom of the model is set to zero. Finally, a constant velocity is applied to the top of the model in the negative z-direction to generate vertical loads on the model. For the on-site uniaxial compression test, 5 MPa, 10 MPa, and 15 MPa were selected as the applied load values in the numerical simulation. The numerical simulation diagrams and data comparison under different load conditions are shown in Table 3.

**Table 3.** Numerical simulation diagrams and data comparison under different load conditions.

By extracting on-site data from uniaxial compression tests and data from numerical simulations, it can be seen that the stress–strain curves of coal samples have similar variation characteristics. The deformation and failure process of coal samples can be divided into three stages: pore compression and elastic deformation stage, plastic deformation stage, and failure and instability stage. And the on-site data and numerical simulation data are basically consistent, proving that the numerical simulation data in this study can be used as a basis for distinguishing the mining stress and overlying rock stress arch of the working face.

### 3.3. The Results of Numerical Simulation

#### (1) Advance support stress distribution

Figure 15 shows the distribution cloud and curve of vertical stress and maximum principal stress during the mining process of longwall panel no. 8102. As shown in the figure, ① longwall panel no. 8102 end overrun coal body stress concentration is obvious, the maximum stress concentration is 27.42 MPa, stress concentration factor is 2.61; ② the two small coal pillars in the 8102 gob are in a state of pressure relief and cannot be carried; ③ the vertical stress of the 8100 gob, 8101 gob, and 8103 gob does not exceed 5 MPa and has not been fully compacted, which confirms the current situation of incomplete mining in a panel and indicates that there are upper hard rock layers bearing it, forming a large structure; ④ the stress concentration of the coal body at the front end is higher on the side close to the 8101 mining area than on the side close to the 8103 working face; ⑤ the direction of the vertical stress vector is relatively close to the direction of the maximum principal stress vector, indicating that the vertical stress becomes the point of maximum principal stress after mining (in the original rock stress state before mining, the horizontal stress is the maximum principal stress map).

#### (2) Distribution of plastic state of coal body

Figure 16 shows the distribution of plastic zones during the mining of the longwall panel no. 8102. As shown in the figure, ① the plastic deformation of the coal body in the longwall panel no. 8102 is the most severe, especially the advanced coal body on one side of the 8101 gob; ② during the mining process of longwall panel no. 8102, the overlying rock forms a C-shaped overlying rock structure, which will exacerbate the degree of mining pressure manifestation in the working face; ③ the maximum plastic principal strain direction of the leading coal body in longwall panel no. 8102 is near horizontal, which

indicates that the middling coal wall is prone to wall spalling during mining; ④ the elastic strain in the gob is relatively high, showing a situation of high strain in the middle and low strain around it, indicating that the Salomon model used has successfully simulated the compaction behavior of the gob.

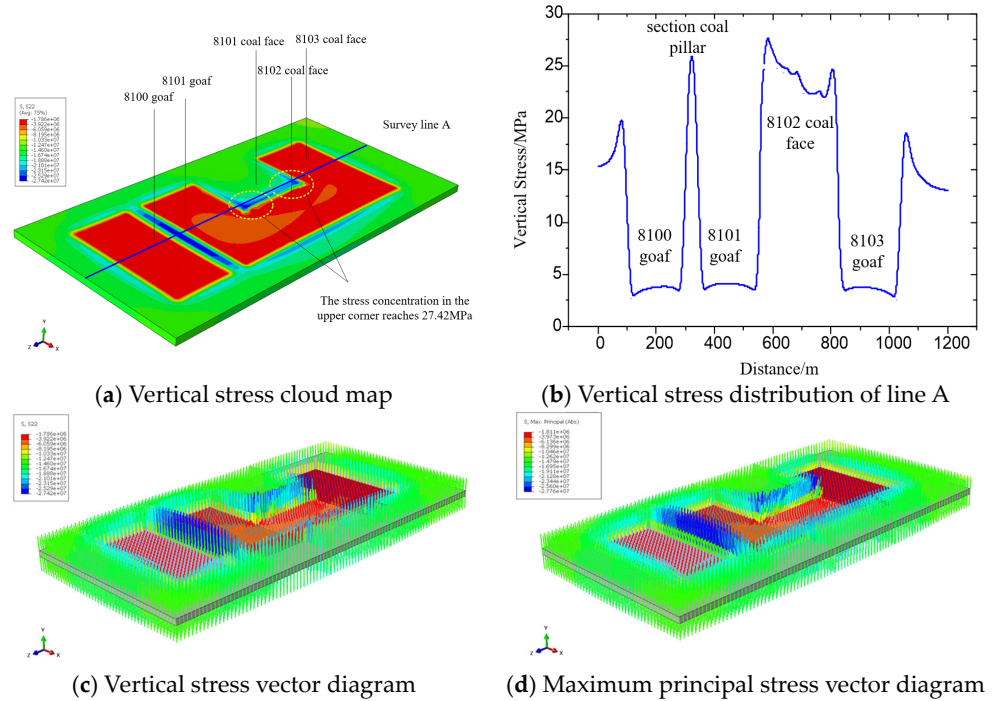


Figure 15. Vertical stress and maximum principal stress distribution diagram.

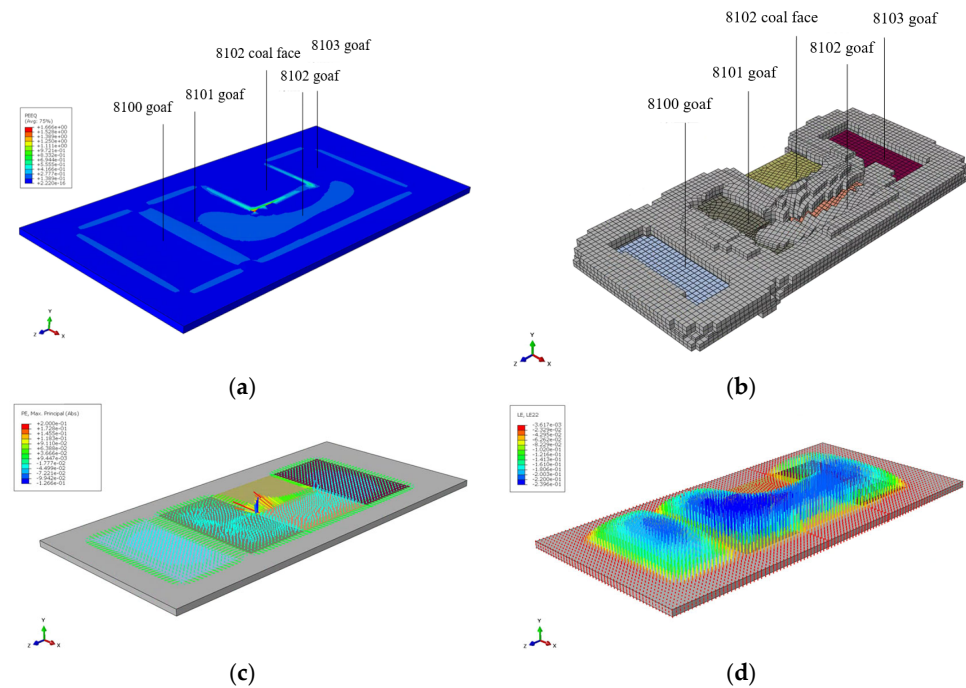


Figure 16. Simulation results of plastic zone distribution during the mining process of longwall panel no. 8102. (a) Distribution of plastic zone. (b) 8102 isolated island working face overlying rock C-shaped structure. (c) Vector plot of maximum plastic principal strain. (d) Vertical strain vector distribution of plasticity.

(3) Analysis of overlying rock stress arch structure

Figure 17 shows the stress cloud for slices at different locations along the working face direction. In the figure, the negative sign represents the rear of longwall panel no. 8102, and the positive sign represents the front of longwall panel no. 8102. From the figure, obviously ① the pressure is relieved behind the longwall panel no. 8102, but it is not fully relieved after 10 m, indicating that this area is affected by the “C”-shaped structure formed by the fracture of the hard top plate; ② the vertical stress is highest at 20 m in front of the working face; ③ stress arch structures with horizontal stress concentrations are formed 50 m above the 8100, 8101, 8102, and 8103 extraction zones, which are interconnected. This stress arch structure will be destroyed with the mining of longwall panel no. 8102, indicating that longwall panel no. 8102 is a key working face. The mining of longwall panel no. 8102 will cause the instability of the entire stress arch structure.

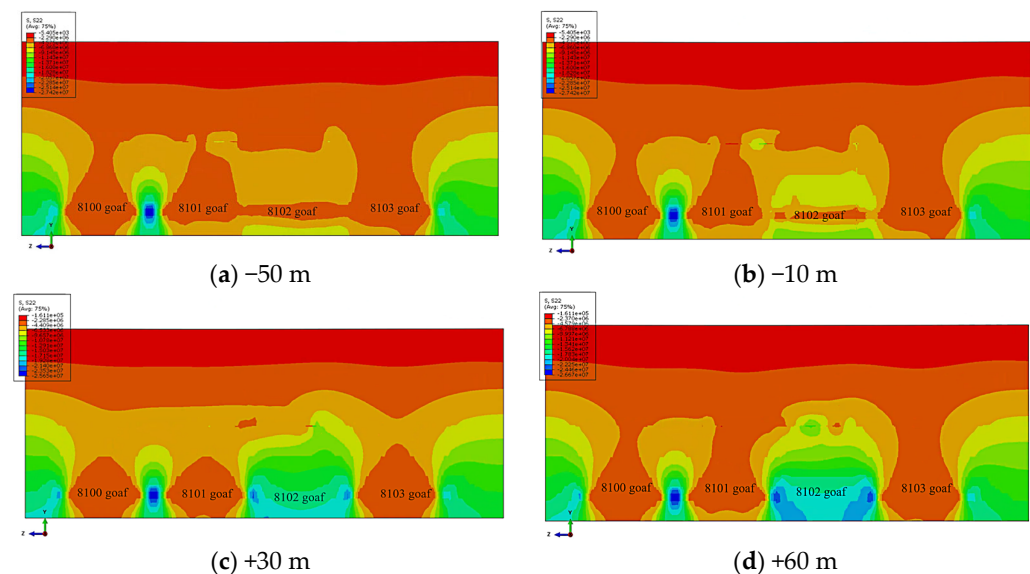


Figure 17. Slice stress cloud maps at different positions along the working face direction.

#### 4. Key Techniques for Hydraulic Fracturing and Pressure Relief of the Roof in the Island Fully Mechanized Caving Face of Extra-Thick Coal Seams

##### 4.1. Safety Risk Analysis of Longwall Panel No. 8102

The longwall panel no. 8102 is an isolated island working face, and the factors that are not conducive to the management of the working face roof and the prevention and control of dynamic phenomena in the working face are as follows:

① The overlying rocks are mostly sandstone layers with high hardness and few cracks, which suddenly break and induce impact loads; ② the mining thickness of the working face is large, the disturbance range of the overlying rock is large, the balance structure of the overlying rock moves upward, and the static load borne by the support is large; ③ on both sides of the longwall panel no. 8102 are gob areas. According to the observation results of surface cracks, there is an asymmetric long-arm suspended sandstone structure overlying the working face; ④ the coal seam is relatively hard and has the possibility of impact.

Therefore, 8102 island working face mining has the risk of strong dynamic pressure on the roof of the working face and rock burst in the coal seam, especially when the working face is first square and second square. In addition to increasing the working resistance of the hydraulic support, a series of technical measures for safety assurance should also be taken, including the pressure relief of the coal body drilling in front of the working face, the pre-cracking of the hard roof plate of the horizontal branch drilling under the well, the dynamic monitoring and early warning of microseisms, the dynamic monitoring of the support status, the dynamic monitoring of the advanced coal body stress, and the corresponding dynamic pressure prevention and control plan measures.

#### 4.2. Pressure Relief Plan for Coal Body Drilling in Front of the Working Face

In order to avoid the risk of sudden fracture of the hard overhanging roof slab rock strata causing impact on the coal body in front of the workings, large-diameter drilling was carried out from two roadways to relieve the pressure of the coal body in front of the workings.

Using a crawler-type drilling rig to drill large-diameter holes in the coal-mining slope construction, the diameter of the drill bit is 200 mm, and after expansion, the diameter is 200 mm. The drilling depth is not less than 120 m, forming a staggered layout of two alleys to eliminate the pressure relief void in the middle of the working face.

The pressure relief drilling construction is carried out in the central area of the coal-mining slope of the roadway, with a horizontal spacing of 900 mm and a vertical spacing of 500 mm between the drilling holes. The opening heights are 1400 mm and 2400 mm, respectively. After the drilling construction is completed, yellow mud is used to seal the hole for 300 mm to prevent gas from overflowing inside the hole. Several observation boreholes can be reserved. The drilling should be scheduled in advance, at least within 100 m of the working face, and the unpressurized drilling arrangement is shown in Figure 18.

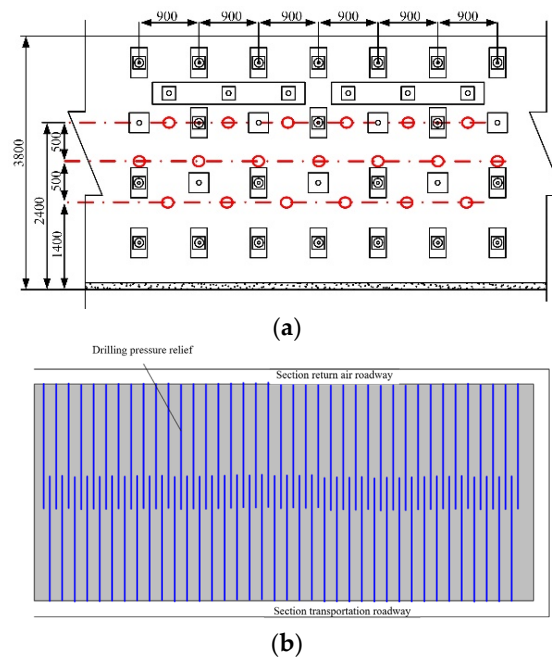


**Figure 18.** Layout of Pressure Relief Drilling in Section 1. (a) Layout of pressure relief drilling holes in the coal mining slope. (b) Interlaced arrangement of drilling holes for construction of two alleys.

#### 4.3. Pre-Splitting of Hard Roof Plate for Horizontal Branch Drilling

##### (1) Analysis of stress field environment of overburden rock in longwall panel no. 8102

In intact hard rock formations, the direction of propagation of hydraulic fractures is most significantly influenced by the ground stress field. Generally, the propagation surface of hydraulic fractures is perpendicular to the direction of the minimum principal stress and towards the direction of the maximum principal stress. The direction of the maximum principal stresses on the roof of the longwall panel no. 8102 has changed considerably due to the influence of the mountain packs on both sides. Figure 19 shows the distribution characteristics of the maximum and minimum principal stress vectors in the longwall panel no. 8102. From Figure 19a, it can clearly be seen that the direction of the maximum principal stress is approximately vertical during the mining of the longwall panel no. 8102, and the maximum principal stress near the end of the working face reaches 24.83 MPa, which is slightly inclined towards the gob. From Figure 19b, it can be seen that the minimum

principal stress direction in the coal body within 180 m of the longwall panel no. 8102 is roughly parallel to the advancing direction of the working face, which makes it easy to form vertical joints parallel to the working face. The minimum principal stress of the coal body 180 m away from the working face is parallel to the inclined direction of the working face, which is due to the release of constraints due to the gob on both sides. In this case, it is easy to form vertical joints parallel to the forward direction of the working face.

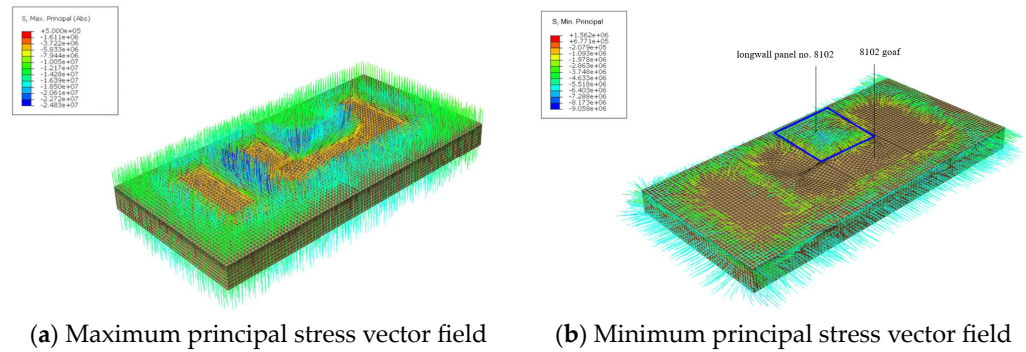


**Figure 19.** Numerical calculation results of maximum and minimum principal stress vector fields in longwall panel no. 8102.

If hydraulic fractures parallel to the working face are to be formed, it is suitable to conduct fracturing within 180 m of the working face in advance. If hydraulic fractures are to be formed parallel to the advancing direction of the working face, it is desirable to fracture within 180 m outside the advancing working face. The hydraulic fractures formed by both fracturing methods are vertical fractures.

(2) Fracturing target layer

There are multiple layers of thick and hard rock layers in the overlying strata of Tongxin Coal Mine, which are the target layers for cracking. The 7 m thick K3 sandstone layer at 454.95 m buried depth, the 17.28 m thick sandy gravel layer at 423.78 m buried depth, the 10.9 m thick sandy gravel layer at 405.40 m buried depth, the 19.3 m thick silty sand layer at 394.5 m buried depth, the 9.55 m thick sandy gravel layer at 366.90 m buried depth, and the 10.95 m thick silty sand layer at 357.35 m buried depth may have a direct impact on the ground pressure of the working face. It is recommended to conduct fracturing in the 17.28 m thick sandy gravel layer at 423.78 m. The initial fracture is formed by perforation, and the perforation location should be within the upper 1/4 of the silty sand layer (as shown in Figure 20), so as to make the rock layer fracture under the action of ground pressure. When this rock layer fractures, the hard rock layer below it will also fracture.

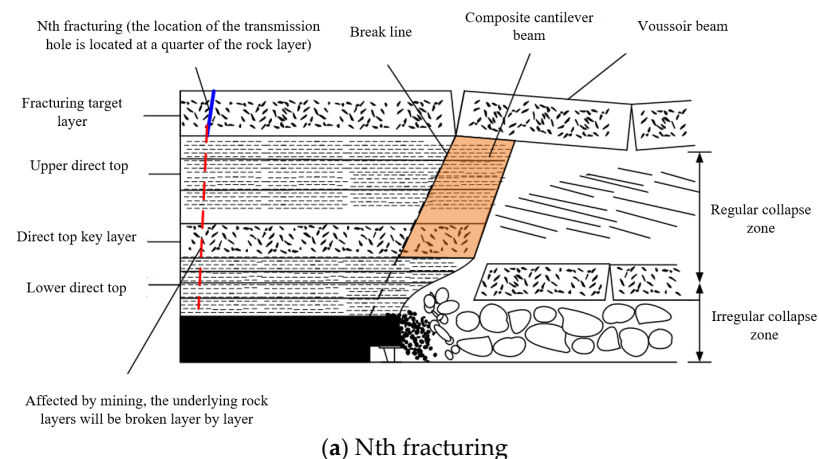


**Figure 20.** Cont.

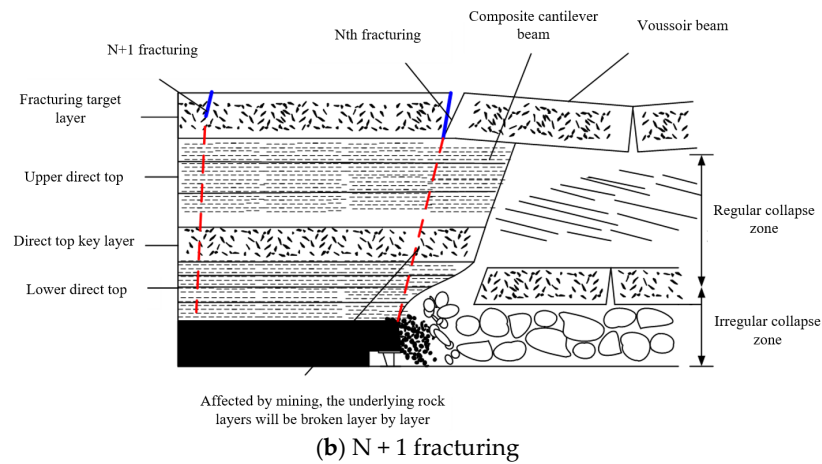
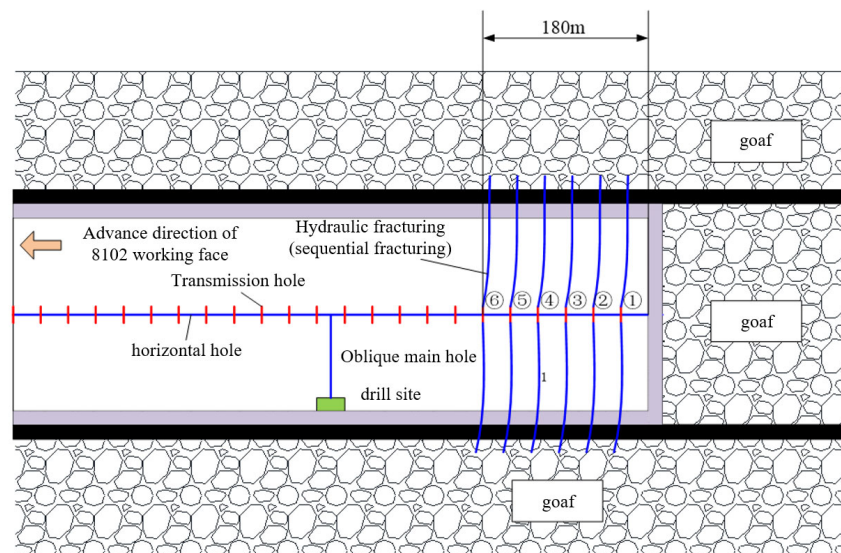


Figure 20. Fracturing target layer and perforation location.

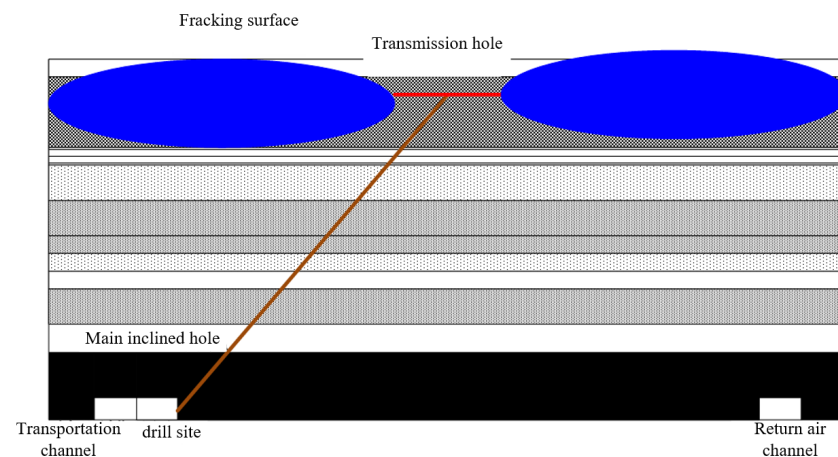
(3) Borehole layout of downhole fracking horizontal branch

In the transportation channel tunnel, starting from the cutting hole, fracturing drilling chambers are drilled every 500 m. The main fracturing hole is drilled diagonally upwards to the 17.28 m thick gravel layer buried at a depth of 423.78 m, which is 2 m from the top surface. The main oblique hole is projected parallel to the working face on the horizontal plane, and the final hole is located in the center of the working face, as shown in Figure 21. Then, horizontal holes are made parallel to the advancing direction of the working face, and the horizontal holes are arranged in this gravel rock layer. Horizontal holes are perforated in sequence with a spacing of 20 m, and then sequential fracturing is used to gradually fracture along the advancing direction from the opening of the cutting hole. To form vertical fractures parallel to the working face, fracturing should always be maintained within 180 m of the working face and should not be carried out in advance. The ultimate goal is to reduce the initial pressure step distance, cut off the cantilever structure of hard rock layers, and reduce the risk of working face impact.



(a) Layout plan of fracking boreholes on roof of longwall panel no. 8102

Figure 21. Cont.



(b) Profile diagram of fracking

**Figure 21.** Layout of fracking boreholes in longwall panel no. 8102.

## (4) Calculation of working resistance of hydraulic support on working face no. 8102

The 3rd to 5th coal seams of Tongxin Coal Mine are extra-thick coal seams with high mining height and integrated mining. The working face no. 8102 is also an isolated island working face in one panel. According to statistical analysis of the rock pressure behavior of other working faces in one panel, it can be concluded that: under the condition of using a 15,000 kN hydraulic support in one panel, it can basically meet the needs of roof management, however, there are still some serious pressure-bearing phenomena, indicating that the 15,000 kN hydraulic support is generally adaptable to the solid coal working face on both sides of the panel or the working face in one side of the air-mining zone. The application of 15,000 kN hydraulic support to the 8102 isolated island working face may face insufficient support resistance. The overlying strata structure of the coal seam is shown in Table 4.

**Table 4.** Structure of overlying strata in coal seams.

Layer Number	Thickness/m	Rock Name	Layer Number	Thickness/m	Rock Name
C1	0.90	Carbonaceous mudstone	C9	10.27	Interbedded mudstone and sandstone
C2	1.80	Coal	C10	2.36	Fine sandstone
C3	4.53	Sandy mudstone	C11	1.90	Glutenite
C4	3.65	Interbedded mudstone and sandstone	C12	17.28	Fine sandstone
C5	7.00	Coarse-grained sandstone	C13	1.10	Glutenite
C6	4.20	Fine sandstone	C14	10.9	Glutenite
C7	3.44	Siltstone	C15	19.30	Siltstone
C8	2	Coal	C16	1.6	Coarse-grained sandstone

The theoretical analysis method was used to determine the working resistance of the 8102 high mining height synthesized stent.

The roof rock layer that meets condition  $\Delta_j - \Delta_m \leq 0$  is the rock layer that needs to be controlled. The top slate layer that meets condition  $\Delta_j - \Delta_m > 0$  is the main roof rock layer.  $\Delta_j$  is the ultimate settlement;  $\Delta_m$  is the possible sinking amount;  $\Delta_m = (h_c + h_f)(1 - p_1) + (1 - k_p)h_m$ ;  $p_1$  is the coal loss rate;  $h_c$  is the coal-cutting height;  $h_f$  is the coal

discharge height;  $k_p$  is the direct crushing expansion coefficient;  $h_m$  is the thickness of a certain continuous roof rock layer.

(1) Determination based on the criteria for controlling rock layers:

$$\begin{aligned}\Delta_{m1} &= 19 \times (1 - 0.2) + (1 - 1.2) \times 0.9 = 15.02 \text{ m} \\ \Delta_{j1} &= h - \frac{ql^2}{2kh[\sigma_c]} < \Delta_{m1}\end{aligned}\quad (19)$$

So, the C1 rock layer is the rock layer that needs to be controlled,

$$\begin{aligned}\Delta_{m2} &= 19 \times (1 - 0.2) + (1 - 1.2) \times 2.7 = 14.66 \text{ m} \\ \Delta_{j2} &= h - \frac{ql^2}{2kh[\sigma_c]} < \Delta_{m2}\end{aligned}\quad (20)$$

So, the C2 rock layer is the rock layer that needs to be controlled,

$$\begin{aligned}\Delta_{m3} &= 19 \times (1 - 0.2) + (1 - 1.2) \times 7.23 = 13.754 \text{ m} \\ \Delta_{j3} &= h - \frac{ql^2}{2kh[\sigma_c]} < \Delta_{m3}\end{aligned}\quad (21)$$

So, the C3 rock layer is the rock layer that needs to be controlled.

By analogy, it is calculated that the C4, C5, C6, C7, C8, C9, C11, C12, and C13 strata are controlled strata, while the C14 stratum and above are the basic roof strata.

(2) Determination of rock layers without deformation pressure:

$$\sum_{i=1}^n (\Delta_j)_i = \Delta_d \quad (22)$$

$\Delta_d$  is the total deformation of the top coal body in the control zone,  $\Delta_d = \eta h_d(1 + \lambda)$ ,  $\eta$  is the porosity, and  $\lambda$  is the lateral pressure coefficient. After calculation, it was found that  $\Delta_d = 6.41$  m, and the C1~C5 rock layers can offset the deformation of the top coal. Therefore, the basic data of C6, C7, ..., C14 are brought into the following equation to calculate the working resistance.

$$P_z = G_d + Q = L_d h_d \gamma + \frac{f \sum_{i=1}^{j+1} P_i (l_i + h_i \cdot ctg\alpha) - 2(Q_B - K \cdot s)(h_{j+1} - \Delta)}{2cf} \quad (23)$$

In consideration of the factor of safety, the maximum value of the static resistance can be obtained, given by

$$P_z = G_d + Q = L_d h_d \gamma + \frac{f \sum_{i=1}^{j+1} P_i (l_i + h_i \cdot ctg\alpha)}{2cf} = 2643.8 + 7789.4 = 11,843.2 \text{ kN} \quad (24)$$

The impact resistance coefficient of the support is taken as 2, which can determine that the working resistance of the hydraulic support should not be less than 20,866.4 kN, and the final value is 21,000 kN.

Appropriately increasing the bracket height of the hydraulic support is conducive to reducing the size of the coal block and improving the capacity of comprehensive release. However, the longwall panel no. 8102 is an isolated island working face. Increasing the mining height increases the working resistance of the stent, even in the case of an integrated working face. Therefore, it is not recommended to increase the height of the support. Therefore, a support height of 3.8 m is adopted, with a support structure height of 2.75~4.2 m.

In summary, ZFY21000/27.5/42 hydraulic support is selected. The working resistance of this type of hydraulic support is 21,000 kN, and it is necessary to pre-crack the roof rock layer in advance and manually create cracks along the working face. The hard roof shall be pre-cracked in advance by means of surface L-shaped horizontal wells or fracking by means of horizontal branch holes under the well.

## 5. Conclusions

- (1) The leading coal body at the end of the longwall working face in an extra-thick coal seam showed significant stress concentration, with a stress concentration coefficient of 2.61. Under the structural characteristics of the strata and the mining conditions in the one-panel area, one side of the hollow workings was mined over for nonsufficient mining and the strata failed to settle sufficiently.
- (2) During the mining process, the overlying strata undergo extensive and intense movement, inducing strong rock pressure. In this case, the structure of the overlying strata undergoes deformation from an asymmetric long-arm “T” before mining into a C-shaped structure during the mining process. The asymmetric T-shaped structure of the hard rock cantilever is located above the working face, causing significant rock pressure after fracture.
- (3) The directional hydraulic fracturing roof control technology was successfully implemented in Tongxin Coal Mine, achieving high stress transfer in the mining roadway of the working face. The appropriate hydraulic support resistance was determined through calculation, and the corresponding hydraulic support was successfully selected.

**Author Contributions:** Methodology, Y.W.; Software, P.C.; Formal analysis, Y.W. and S.W.; Resources, S.W. All authors have read and agreed to the published version of the manuscript.

**Funding:** This study was supported by the National Natural Science Foundation of China (No. 52204090).

**Data Availability Statement:** Not applicable.

**Conflicts of Interest:** The authors declare no conflict of interest.

## References

1. Ren, X.; Hao, B.; Wang, H.; Zhao, J.; Zhang, J.; Zhang, C. Roadway Protection by Roof-Cutting in the Support Removing Channel of the Long-Wall Mining Face. *Shock Vib.* **2022**, *2022*, 8116399. [[CrossRef](#)]
2. Gao, M.; He, Y.; Xu, D.; Yu, X. A New Theoretical Model of Rock Burst-Prone Roadway Support and Its Application. *Geofluids* **2021**, *2021*, 5549875. [[CrossRef](#)]
3. Wang, P.; Zhang, N.; Kan, J.; Xu, X.; Cui, G. Instability Mode and Control Technology of Surrounding Rock in Composite Roof Coal Roadway under Multiple Dynamic Pressure Disturbances. *Geofluids* **2022**, *2022*, 8694325. [[CrossRef](#)]
4. Yang, H.; Zhang, N.; Han, C.; Sun, C.; Song, G.; Sun, Y.; Sun, K. Stability Control of Deep Coal Roadway under the Pressure Relief Effect of Adjacent Roadway with Large Deformation: A Case Study. *Sustainability* **2021**, *13*, 4412. [[CrossRef](#)]
5. Yang, Z.-Q.; Liu, C.; Jin, H.-W. Study on Pressure Relief Zone Formed Inside Roadway Rib by Rotary Cutting with Pressurized Water Jet for Preventing Rock Burst. *Adv. Civ. Eng.* **2022**, *2022*, 9647029. [[CrossRef](#)]
6. Yang, X.; Hu, C.; He, M.; Wang, H.; Zhou, Y.; Liu, X.; Zhen, E.; Ma, X. Study on Presplitting Blasting the Roof Strata of Adjacent Roadway to Control Roadway Deformation. *Shock Vib.* **2019**, *2019*, 3174898. [[CrossRef](#)]
7. Chen, X.; Wang, X.; Zhang, D.; Qin, D.; Wang, Y.; Wang, J.; Chang, Z. Creep and Control of the Deep Soft Rock Roadway (DSRR): Insights from Laboratory Testing and Practice in Pingdingshan Mining Area. *Rock Mech. Rock Eng.* **2022**, *55*, 363–378. [[CrossRef](#)]
8. Ji, M.; Guo, H. Influence of In-Situ Rock Stress on the Stability of Roadway Surrounding Rock: A Case Study. *J. Geophys. Eng.* **2020**, *17*, 138–147. [[CrossRef](#)]
9. Yuan, Y.; Han, C.; Zhang, N.; Feng, X.; Wang, P.; Song, K.; Wei, M. Zonal Disintegration Characteristics of Roadway Roof Under Strong Mining Conditions and Mechanism of Thick Anchored and Trans-Boundary Supporting. *Rock Mech. Rock Eng.* **2022**, *55*, 297–315. [[CrossRef](#)]
10. Qian, D.; Deng, J.; Wang, S.; Yang, X.; Cui, Q.; Li, Z.; Jin, S.; Liu, W. Deformation Characteristics and Control Countermeasures for Surrounding Rock of Deep Roadway under Mining Disturbance: A Case Study. *Shock Vib.* **2022**, *2022*, 9878557. [[CrossRef](#)]
11. Wang, K.; Wang, L.; Ren, B.; Fan, H. Study on Seepage Simulation of High Pressure Grouting in Microfractured Rock Mass. *Geofluids* **2021**, *2021*, 6696882. [[CrossRef](#)]

12. Cheng, Y.; Bai, J.; Ma, Y.; Sun, J.; Liang, Y.; Jiang, F. Control Mechanism of Rock Burst in the Floor of Roadway Driven along Next Gob in Thick Coal Seam with Large Obliquity Angle in Deep Well. *Shock Vib.* **2015**, *2015*, 750807. [[CrossRef](#)]
13. Jolfaei, S.; Lakirouhani, A. Sensitivity Analysis of Effective Parameters in Borehole Failure, Using Neural Network. *Adv. Civ. Eng.* **2022**, *2022*, 4958004. [[CrossRef](#)]
14. Yang, J.; Liu, C.; Yu, B. Application of Confined Blasting in Water-Filled Deep Holes to Control Strong Rock Pressure in Hard Rock Mines. *Energies* **2017**, *10*, 1874. [[CrossRef](#)]
15. Gao, R.; Yu, B.; Meng, X. Stress Distribution and Surrounding Rock Control of Mining near to the Overlying Coal Pillar in the Working Face. *Int. J. Min. Sci. Technol.* **2019**, *29*, 881–887. [[CrossRef](#)]
16. Chen, L.; Li, Q.; Yang, J.; Qiao, L. Laboratory Testing on Energy Absorption of High-Damping Rubber in a New Bolt for Preventing Rockburst in Deep Hard Rock Mass. *Shock Vib.* **2018**, *2018*, 7214821. [[CrossRef](#)]
17. Jiang, F.X. Viewpoint of Spatial Structures of Overlying Strata and Its Application in Coal Mine. *J. Min. Saf. Eng.* **2006**, *23*, 30–33.
18. Salamon, M.D.G. Mechanism of caving in longwall coal mining. In Proceedings of the 31st U.S. Symposium of Rock Mechanics, Golden, CO, USA, 18–20 June 1990; West Virginia University Press: Morgantown, WA, USA, 1990.
19. Wang, H.; Poulsen, B.A.; Shen, B.; Xue, S.; Jiang, Y. The influence of roadway backfill on coal pillar strength by numerical investigation. *Int. J. Rock Mech. Min. Sci.* **2011**, *48*, 443–450. [[CrossRef](#)]

**Disclaimer/Publisher’s Note:** The statements, opinions and data contained in all publications are solely those of the individual author(s) and contributor(s) and not of MDPI and/or the editor(s). MDPI and/or the editor(s) disclaim responsibility for any injury to people or property resulting from any ideas, methods, instructions or products referred to in the content.